

Earthquake Processes in the Long Valley Caldera Area, California

BRUCE R. JULIAN

U.S. Geological Survey, Menlo Park, California

STUART A. SIPKIN

U.S. Geological Survey, Denver, Colorado

At least three large earthquakes in 1978 and 1980 near Long Valley caldera have unusual non-double-couple mechanisms, unlike those appropriate for shear faulting. This conclusion is supported by short-period *P* first motions, long-period *P* and *SH* first motions, surface wave spectral amplitudes and initial phases, and long-period *P* and *SH* waveforms. Two explanations for these anomalous mechanisms have been proposed: (1) simultaneous strike slip and normal motion on separate faults and (2) tensile failure under high fluid pressure. To evaluate these conflicting hypotheses, we have inverted *P* and *SH* waveforms recorded by the Global Digital Seismograph Network (GDSN) to obtain moment tensors for the earthquakes and have also generated broadband seismograms by deconvolving short- and long-period GDSN data. The largest event (1633:44 UTC, May 25, 1980) has a duration of about 20 s and can be resolved into three events, separated by intervals of about 7 and 10 s, each having a non-double-couple mechanism. This contrasts with previously reported inversion results for other complex earthquakes, all of which have double-couple subevents. Furthermore, the earthquake of 1450:56 UTC May 27, 1980, appears to be simple and not composed of smaller events. Thus the non-double-couple mechanisms are probably intrinsic to the source process and not artifacts caused by misinterpretation of multiple ruptures as single events. Rapid opening of cracks under high fluid pressure is a likely possibility for this process, although its dynamics are complex and not yet fully understood.

INTRODUCTION

Since October 1978, Long Valley caldera has experienced four earthquakes in the magnitude 6 range and several earthquake swarms involving thousands of smaller events. The most intense activity occurred from May 25 to May 27, 1980, when four of the largest earthquakes occurred, but even today, 6 years after the earthquakes began, Long Valley remains the most seismically active area in California. This unusual activity, coupled with geodetically detected uplift within the caldera, has aroused fears of a possible volcanic eruption, and has led the U.S. Geological Survey to issue a formal "notice of volcanic hazard" for the area.

Figure 1 is a map of the Long Valley area, showing the epicenters of earthquakes in 1980 larger than magnitude 4. The three largest earthquakes in 1980 and the Wheeler Crest earthquake of October 4, 1978 are identified on Figure 1, and their locations and other parameters are given in Table 1. Another large earthquake, at 1649:26 UTC, May 25, 1980, has been omitted and is not analyzed in this paper because its seismic waves are seriously contaminated by those from event 1. R. Cockerham determined the hypocenters and origin times given in Table 1, using local and regional arrival times recorded by the U.S. Geological Survey, the California Institute of Technology, and the University of Nevada. The magnitudes were computed by the International Seismological Centre and were taken from that agency's bulletin. The focal mechanism shown for the Wheeler Crest earthquake was computed by *Ekström and Dziewonski* [1983]. The mechanisms for events 1–3 were derived in this study by waveform inversion and are discussed in more detail below. Different types of data and analysis methods were used to derive the seismic moments in Table 1; Table 1 shows the approximate periods of the waves

used. The moments determined in this study will be discussed in more detail in a later section.

For the largest earthquakes, unusually complete data are available because there are more than 500 short-period seismometers in California and western Nevada and because the earthquakes were large enough to generate well-observed teleseismic waves. These data have, however, proved difficult to interpret. Mechanisms derived by applying conventional seismological methods to different subsets of the data are inconsistent with each other, as though the data were internally inconsistent [*Given et al.*, 1982]. Two possible reasons for this difficulty have been suggested. First, spatial or temporal complexity of the rupture process may have led to spurious results when the earthquakes were modeled as simple point sources. In particular, *Ekström* [1983] and *Wallace et al.* [1983] attribute the anomalous earthquakes to simultaneous dip-slip and strike-slip motion on different faults. Second, seismic wave propagation anomalies caused by complex earth structure in the area may have biased the analysis. A much simpler possibility, however, is that the earthquakes have mechanisms whose equivalent force systems are not pure double couples. The difficulty in interpreting the data disappears if a general moment tensor source representation is used instead of the conventional but more restrictive double-couple force system [*Julian*, 1983; *Barker and Langston*, 1983; *Ekström and Dziewonski*, 1983]; all the different types of data, covering a three-decade frequency band, can then be explained by similar mechanisms with large compensated linear vector dipole (CLVD) components [*Knopoff and Randall*, 1970]. In fact, there may be geological reasons to expect such mechanisms in volcanic areas. *Julian* [1983] suggested that they might be a consequence of tensile failure under high fluid pressure, such as would accompany dike intrusion. It is obviously important to resolve this disagreement, both to evaluate the potential volcanic hazard at Long Valley and to advance our understanding of seismic and volcanic processes.

In this paper, we examine the available seismological data

This paper is not subject to U.S. copyright. Published in 1985 by the American Geophysical Union.

Paper number 4B5209.

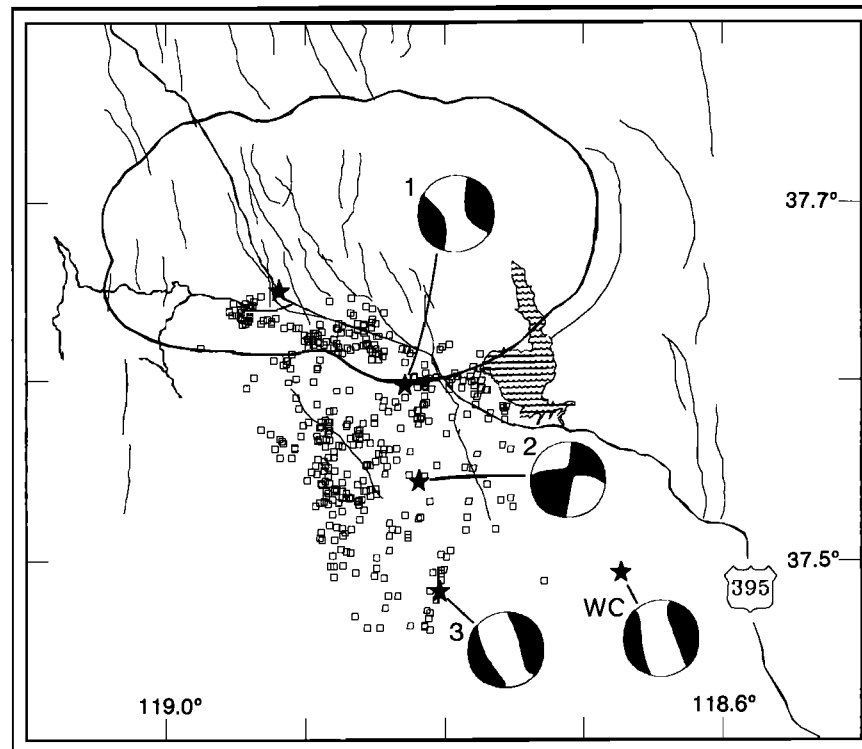


Fig. 1. Long Valley caldera and vicinity, showing best located earthquakes in 1980 larger than magnitude 3. Numbered focal spheres: mechanisms obtained in this study for events 1–3. WC, mechanism derived by *Ekström and Dziewonski* [1983] for Wheeler Crest earthquake of October 4, 1978. Star without focal sphere is epicenter of earthquake of 1649:26 UTC, May 25, 1980. Heavy lines, caldera boundary and highways. Light lines, normal faults.

for the Long Valley earthquakes (short-period P wave motions, long-period P and SH wave first motions, long-period P and SH waveforms, and long-period surface wave amplitudes and phases). We analyze the digitally recorded P and SH waveforms in the most detail because such data can best resolve the geometrical and temporal characteristics that are diagnostic of multiple events.

PREVIOUS STUDIES

Field Observations

Surface ruptures in the earthquakes of May 1980 [Taylor and Bryant, 1980; Clark *et al.*, 1982] were distributed in a

north-northwest trending region about 20 km long and up to 10 km wide within Long Valley caldera and extending south-eastward from the caldera along the Hilton Creek fault. The pattern of fractures was complex, involving both normal faulting (down to the northeast, usually) and tensional cracking (relative displacements east-west to northeast-southwest) on numerous branching traces, mostly unrelated to known faults, and undoubtedly often complicated by ground failure caused by shaking. Extensional cracking seems to have been the dominant type of faulting. The 82 measurements tabulated by Taylor and Bryant include 25 cases in which vertical offset dominated, 52 cases where extension dominated, and five cases in which vertical and extensional offsets were about

TABLE 1. Earthquakes Studied

Event	Origin Time		Latitude N	Longitude W	Depth, km	Magnitude		$M_{0(\text{Period})}$, 10^{18} N m
	Date	UTC				m_b	M_s	
Wheeler Crest	Oct. 4, 1978	1642:48.3	37.49°	118.67°	7	5.3	5.3	0.18 _(>4.5) (ED)
1	May 25, 1980	1633:44.2	37.60°	118.83°	8	6.1	6.1	2.9 _(1.50) (GWK) 1.87 ₍₂₀₎ (BL) 1.8 _(>4.5) (ED) 2.3 ₍₂₅₎ (JS)
2	May 25, 1980	1944:50.7	37.54°	118.82°	7	5.6	6.0	1.3 ₍₈₀₎ (GWK) 0.8 _(>4.5) (ED) 1.2 ₍₂₅₎ (JS)
3	May 27, 1980	1450:56.5	37.48°	118.80°	10	5.7	6.0	1.1 ₍₈₀₎ (GWK) 1.03 ₍₂₀₎ (BL) 0.8 _(>4.5) (ED) 1.3 ₍₂₅₎ (JS)

GWK, *Given et al.* [1982]; BL, *Barker and Langston* [1983]; ED, *Ekström and Dziewonski* [1983]; JS, this study.

equal. The largest displacements (both vertical and extensional) were about 25 cm, but most were much smaller. Strike-slip offset was a minor component of the faulting, observed in only a few places, and was right-lateral on north to northwest trending faults.

Previous Seismological Studies

Several investigators have studied the mechanisms of the largest Long Valley earthquakes seismologically, but their conclusions do not agree. This disagreement arises because the seismological data require mechanisms with large non-double-couple components.

The first seismological studies [*Cramer and Topozada*, 1980; *Ryall and Ryall*, 1981] were based primarily on first motions of short-period *P* waves recorded on seismographs in California and Nevada. These waves have first motions displaying an apparently quadrantal pattern (though most of the waves have takeoff angles from about 50°–90° and sample the center of the lower focal hemisphere poorly), which was interpreted as evidence of strike-slip motion on nearly vertical faults. However, neither of the two possible interpretations, involving either left-lateral motion on north-south faults or right-lateral motion on east-west faults, is supported by the field observations described above.

These strike-slip interpretations were called into question by a later study of the amplitudes and initial phases of 80- to 200-s surface waves recorded by the Global Digital Seismograph Network [*Given et al.*, 1982]. The Rayleigh waves do not have the symmetric four-lobed radiation pattern expected for strike-slip mechanisms but are largest in the directions N68°E and S68°W and small in the perpendicular directions, much as they are for normal-faulting earthquakes. *Given et al.* inverted the surface wave data to determine the moment tensor for the largest earthquake (event 1). For the periods they considered (150–200 s) the event was effectively at the free surface, so that three components of the moment tensor, M_{xx} , M_{yy} , and M_{zz} , could not be determined. (The *z* axis is taken to be vertical.) *Given et al.* therefore imposed the constraints $M_{zz} = -M_{xx} - M_{yy}$ (no net volume change) and $M_{xz} = M_{yz} = 0$. The inversion procedure yielded a moment tensor that can be represented as a combination of three orthogonal force dipoles: a vertical compressional dipole with a moment of 1.33×10^{18} N m, a horizontal compressional dipole oriented N22°W with a moment of 1.35×10^{18} N m, and a horizontal extensional dipole oriented N68°E with a moment of 2.68×10^{18} N m. This mechanism is not a double couple; to well within the probable observational errors, it is a pure CLVD. *Given et al.* [1982] then took advantage of the indeterminacy of the mechanism and added M_{xz} and M_{yz} components to the moment tensor to obtain a double-couple solution, which they interpreted as left-lateral oblique normal slip on a fault plane striking N12°E and dipping 50°E. As they acknowledged, however, this double-couple mechanism is inconsistent with short-period first-motion observations.

Barker and Langston [1983], *Julian* [1983], and *Ekström and Dziewonski* [1983] independently noticed that the apparent inconsistencies in the seismological data do not exist if a general moment tensor source is allowed. In fact, in their study of long-period body wave waveforms recorded by the World-Wide Standardized Seismograph Network (WWSSN), *Barker and Langston* [1983] found that the non-double-couple moment tensors derived by inverting long-period body wave waveforms explain nearly all the *P* wave first-motion observations, even though no such data were used in the inversions.

The mechanisms they derived for events 1 and 3 have nondouble components amounting to 61.6 and 61.1% of their total moments. (There are several ways to decompose the deviatoric part of a moment tensor into double-couple and CLVD components, and the result depends strongly on which method is used. In this paper we use the decomposition scheme of *Knopoff and Randall* [1970], for which the primary axis of the CLVD is made to coincide with either the *P* or *T* axis of the double couple, as would be expected if the two components of the mechanism are responding to the same stress field. *Barker and Langston* used a different method, which gave values of 36.5 and 36.1% for the two events. Other methods give CLVD components as large as 84%.)

Effects of Complex Structure

Several investigators [*Given et al.*, 1982; *Wallace et al.*, 1982; *Barker and Langston*, 1983] have suggested that the difficulty in explaining the seismological observations using double-couple sources is caused by anomalous wave propagation through complex structures associated with Long Valley caldera or the eastern front of the Sierra Nevada, but no quantitative hypotheses about such effects have been advanced. In addition to the fact that the difficulty disappears if non-double-couple mechanisms are allowed, several other lines of evidence argue against an explanation in terms of anomalous wave propagation.

The 1978 Wheeler Crest earthquake and events 1 and 3 all have similar non-double-couple mechanisms, even though they are different distances from both the caldera and the Sierra Nevada range front and cannot plausibly be supported to have undergone identical propagation effects. The Wheeler Crest earthquake is within about 3 km of the range front and about 15 km from the caldera, whereas event 1 is within 2 km of both the range front and the caldera boundary, and event 3 is 13 km from the range front and 15 km from the caldera. Even more difficult to explain as a wave propagation effect, event 2, which is located in the midst of the three non-double-couple events referred to above, has a double-couple mechanism, as we will show in a later section.

Furthermore, the pattern of anomalies required is not compatible with plausible structures in the area. The surface waves analyzed by *Given et al.* [1982] have wavelengths of 700 km or more and would not be affected significantly by a caldera 30 km in diameter. Therefore, if the mechanism (of event 1, for example) is a double couple, it must have an oblique slip mechanism like that proposed by *Given et al.*, that is consistent with the surface wave observations, and it must be the shorter-period *P* waves that are strongly distorted by complex structures. In particular, the focal sphere plot (Figure 2) shows that waves leaving the source in southerly and northeasterly directions must have apparent positions on the focal sphere that have been moved 20° or 30° toward the southwest. For the northerly rays, such an anomaly might conceivably be attributed to refraction around a low-velocity region beneath the southeastern corner of the caldera, although there is no other evidence for the existence of such a feature. The southerly rays would require a low-velocity region beneath the Sierra Nevada. What is known of the crustal and upper mantle structure in the region, however, suggests that seismic velocities are, if anything, higher beneath the Sierra Nevada than they are further east. For example, seismic refraction measurements [*Eaton*, 1963; *Johnson*, 1965] show that the compressional wave speed at the top of the mantle is about 7.9 km/s beneath the Sierra Nevada and 7.8 km/s beneath the

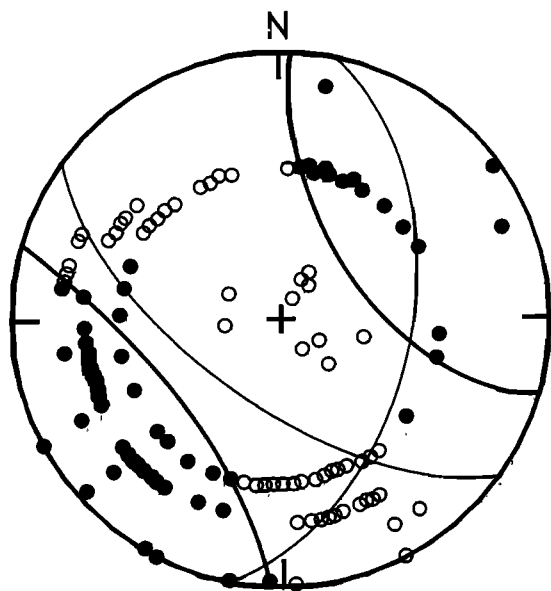


Fig. 2. Short-period P wave first motions for earthquake 1. Data from Figure 5b of *Given et al.* [1982]. Lower focal hemisphere is shown in equal-area projection. Solid circles, compressions; open circles, dilatations. Light curves, nodal planes for shear fault with strike 12° , dip 50° , and rake -35° , as proposed by *Given et al.* [1982]; heavy curves, nodal surfaces for mechanism fitted to these data (80% CLVD, 20% double couple; principal moments in the ratio 2: -1.2: -0.8 with primary axis extensional and trending $N55^\circ E$ and plunging 7.5°).

Basin and Range province. Furthermore, changes in crustal thickness seem inadequate to produce the required effect. Both of the above-mentioned studies conclude that the crustal root of the Sierra Nevada continues eastward at least as far as the California-Nevada border, well to the east of the region traversed by the waves in question.

Simultaneous Multiple Ruptures

A possibility suggested by both *Barker and Langston* [1983] and *Ekström* [1983] is that the double-couple mechanisms may be artifacts caused by complex ruptures. If two double couples with different orientations are superposed, the resultant force system is, in general, not a double couple. (Conversely, the deviatoric part of any non-double-couple force system can be decomposed into a pair of double couples; there are infinitely many ways to perform such a decomposition.) Therefore, if two shear-faulting earthquakes happen at nearly the same time, the resultant point source derived from long-period seismic data can have a non-double-couple component. In particular, a combination of a strike-slip fault and a normal fault, both having horizontal tension axes trending about $N65^\circ E$, might be mistaken for a non-double-couple mechanism similar to those observed. Such simultaneous events are unlikely to occur accidentally; it is extremely improbable that three of the large Long Valley earthquakes involved such chance occurrences. If the anomalous events are simultaneous slip on multiple faults, they must be caused by some unusual process.

A much simpler possibility, suggested by *Julian* [1983], is that the earthquakes are caused not by slip on faults but by tensile failure under high fluid pressure. This process has a non-double-couple equivalent force system and, as mentioned above, might be expected to occur in volcanic areas. Only six adjustable parameters (five moment tensor components and

focal depth) are needed to specify such a source, whereas a pair of double-couple earthquakes requires 12 (eight moment tensor components, two focal depths, and the two components of the epicentral difference). The purpose of this paper is to try to decide between the alternative hypotheses of (1) simultaneous shear-faulting earthquakes and (2) tensile failure, as explanations of the anomalous earthquakes.

BODY WAVE FIRST MOTIONS

Short-Period P Waves

Figures 2 and 3 show the observed first motions of short-period P waves for events 1 and 3. These data were taken from Figures 5b and 10 of *Given et al.* [1982], and most of them came originally from seismograph networks operated in California and Nevada by the U.S. Geological Survey, the University of Nevada, and the California Institute of Technology. The teleseismic data came originally from the Earthquake Data Reports (EDR) of the U.S. Geological Survey. Also shown in Figures 2 and 3 are the nodal planes corresponding to the double-couple mechanisms proposed by *Given et al.* [1982] as well as the nonplanar nodal surfaces corresponding to non-double-couple mechanisms fitted to the data (see figure captions). As can be seen, the non-double-couple mechanisms fit the short-period first motions much better than the double couples: they have only four and two inconsistent data for the two events, whereas the double couples have 32 and 16.

The conventional graphical method of determining fault plane solutions, using a stereographic or equal-area net, can not usually be applied to non-double-couple mechanisms. Therefore the mechanism shown in Figure 2 for event 1 was determined by a recently developed technique that uses linear programming methods to determine seismic focal mechanisms from polarity observations [*Julian*, 1985]. Since the mechanism for event 3 (Figure 3) is a pure CLVD with its primary principal axis horizontal, it was possible to determine it by hand.

To check the reliability of the short-period first motions, we have examined most of the seismograms on which they are

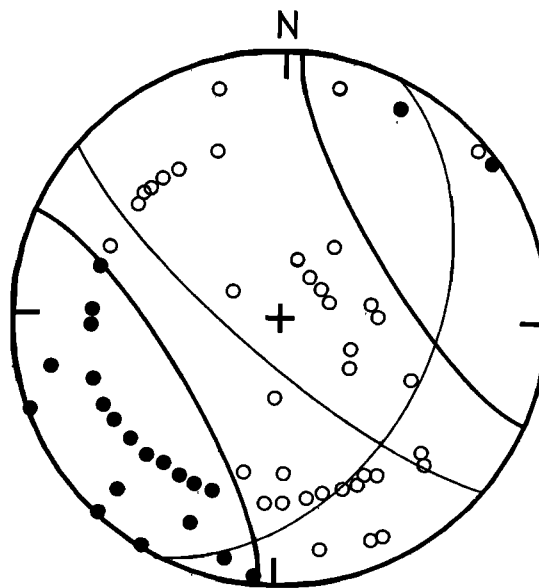


Fig. 3. Same as Figure 2 for earthquake 3. Data from Figure 10 of *Given et al.* [1982]. Shear fault has strike 25° , dip 42° , and rake -19° . Heavy curve is for hand-fitted CLVD with horizontal primary axis trending $N58^\circ W$.

based. On short-period seismograms, event 1 began more impulsively and provides more reliable first motions than does event 3. Furthermore, for both events the compressional first motions are more impulsive and reliable than the dilatational ones. The most reliable dilatational first motions are those observed at U.S. Geological Survey stations near Walker Pass and the southern Owens Valley. It is interesting to note that first motions for rays leaving the source in a west-northwesterly direction, roughly tangent to the southern boundary of the caldera, do not agree with the predictions for either double-couple or non-double-couple mechanisms. This may be an effect of wave propagation through a region of complex structure.

Lide and Ryall [1984] have criticized interpretations based on both regional and teleseismic short-period first motions because the two data sets may not refer to the same part of the source time function. The regional first motions may refer to a small initial event and the teleseismic observations to a larger event slightly later. These events must occur within about 1 s of each other because the reported arrival times at regional and teleseismic distances are consistent (see, for example the bulletin of the International Seismological Centre). In support of their criticism, Lide and Ryall presented broadband seismograms of earthquakes 1 and 3 and of one aftershock from each, recorded at the U.S. Forest Service Visitor Center at Mammoth Lakes, at epicentral distances of about 11 km from earthquake 1 and 22 km from earthquake 3. They interpreted later arrivals on these seismograms as evidence that both earthquakes 1 and 3 began as small events, followed within about 0.25 s by larger events. Comparison of the seismograms with strong motion records obtained closer to the earthquakes and with the numerous local and regional seismograms supports this interpretation for earthquake 3 but suggests that the later arrivals for earthquake 1 are probably not separate events but rather are caused by propagation effects. The local and regional seismograms of earthquake 3, as well as the strong motion seismogram displayed by Hartzell [1982] (discussed in more detail below), all show the onset to be small and followed by larger later arrivals. If, as seems probable, this pattern truly reflects the source time function, then the correctness of the first-motion interpretation depends on whether the subevents had significantly different mechanisms. The *P* wave polarities for the presumed subevents appear to be consistent, both on the broadband seismogram of Lide and Ryall and on the local and regional seismograms, although polarities of later arrivals are of course difficult to determine. Thus earthquake 3 probably does begin with a small event, but it is not clear whether this fact invalidates the interpretation of its short-period first motions. For earthquake 1, on the other hand, most of the local and regional short-period seismograms have onsets much larger than those for earthquake 3 and do not show evidence of a larger event within the first second or two. About 0.3 s after the *P* wave of earthquake 1 on Lide and Ryall's broadband seismogram, there is a second arrival, which they interpreted as a second, somewhat larger, earthquake. However, the seismogram of the aftershock has a similar second arrival, which suggests that these arrivals may be caused by multipath propagation rather than being separate earthquakes. The ray paths involved cross the southern boundary of the caldera at a small angle, a situation in which complex propagation effects are to be expected. In any case, the evidence from local and regional seismograms is equivocal because many records are clipped after the first few cycles, and it is difficult to distinguish source effects from complex propagation effects at regional distances.

Better evidence about the source time function of earthquake 1 is provided by the closest seismograph that recorded it, a strong-motion instrument at Convict Creek at an epicentral distance of less than 2 km. The seismograms for earthquakes 1 and 3 and for an aftershock near earthquake 1 are shown by Hartzell [1982], who modeled the seismogram for earthquake 1 by superimposing delayed and scaled seismograms from earthquake 3 and the aftershock. The seismogram for earthquake 1 is complex, having a long duration and consisting of two events of roughly comparable size about 4–6 s apart and with intervening events being considerably smaller. (This interpretation was suggested originally by Given *et al.* [1982] and agrees with Hartzell's modeling of the seismograms and the long-period body wave inversion results of both Barker and Langston [1983] and this study, discussed below.) The *S* wave onset (the *P* wave was not recorded) is abrupt and larger than any later arrivals for at least 4 s. It is thus likely that the regional and teleseismic short-period first motions refer to the same part of the rupture process. Nevertheless, the short-period first motions are certainly the least reliable of the various data sets. The most satisfactory way to interpret the short-period waveforms would be to compare them with ones calculated from dynamic models of the source process, as will be discussed in more detail below.

Long-Period *P* and *SH* Waves

Long-period *P* and *SH* wave first motions are shown in Figure 4. Most of these data come from the WWSSN and the Global Digital Seismograph Network (GDSN). Also shown in Figure 4 are nodal surfaces for the double-couple mechanism proposed by Given *et al.* [1982] and for a non-double-couple mechanism determined by the linear programming method mentioned above. The non-double-couple mechanism fits the data better than the double couple, with the difference being most pronounced for the *SH* data. Furthermore, the linear programming analysis demonstrates that these long-period first motions are incompatible with a double-couple mechanism.

Nodal Surface Geometry

The nodal surfaces plotted on the focal sphere in Figures 2, 3, and 4 bear little resemblance to the more familiar ones that are appropriate for double couples. To help clarify the difference between the patterns for double-couple and non-double-couple sources, Figure 5 shows the geometry of the nodal surfaces for a pure double couple and a pure CLVD. For a double couple the surfaces are orthogonal planes whose intersections with the focal sphere are orthogonal great circles that divide the focal sphere into equal quadrants. For a CLVD, on the other hand, the surfaces are circular cones, whose intersections with the focal sphere are two small circles that divide the focal sphere into three regions. The Japanese, who first considered mechanisms of this kind referred to them as of "conical type" [Ishimoto, 1932]. (The apex angles of these cones are $\cos^{-1}(-1/3) = 109.47^\circ$, the "tetrahedral angle.") For mechanisms intermediate between double couples and CLVD's, the nodal surfaces are more general (not circular) cones; the planar surfaces for a double couple may be considered as limiting cases of such cones, corresponding to the case when one principal moment is zero.

WAVEFORM INVERSION

Probably the most powerful method for obtaining detailed information about earthquake mechanisms and time functions is to invert high-resolution digital waveforms of body waves to

LONG-PERIOD FIRST MOTIONS

25 May 1980 1633:44

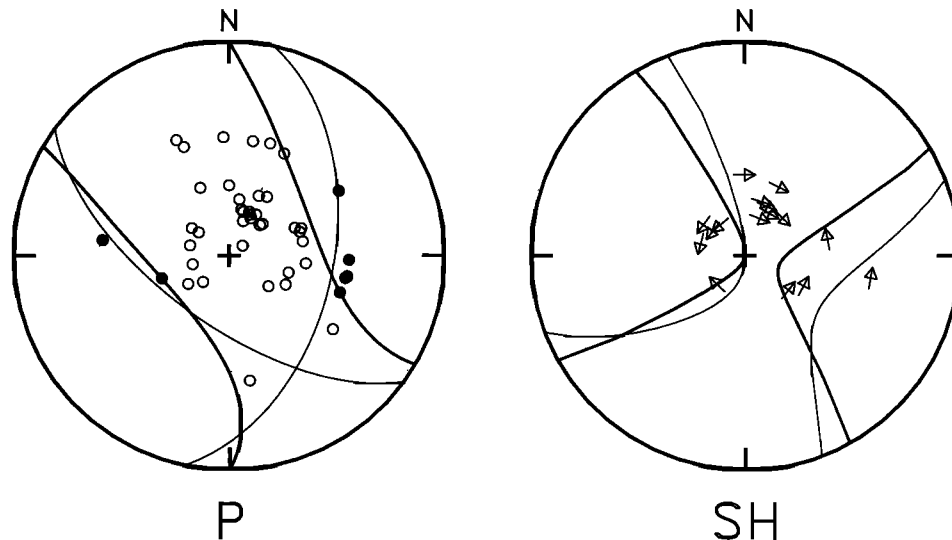


Fig. 4. Long-period P and SH wave first motions for earthquake 1. Solid circles, compressions; open circles, dilations. Light curves, nodal surfaces for shear fault with strike 12° , dip 50° , and rake -35° , as proposed by *Given et al.* [1982]; heavy curves, nodal surfaces for moment tensor fitted to these data (see text).

estimate the parameters in a moment tensor source representation. We did this for three of the earthquakes of May 1980, applying the multichannel signal enhancement (MSE) and multichannel vector deconvolution (MVD) algorithms [Oldenburg, 1982; Sipkin, 1982] to long-period P and SH waveforms recorded by the Global Digital Seismograph Network (GDSN). Although the two methods differ in their mathematical details, they produced similar results. Moreover, res-

olution estimates provided by the MVD algorithm show that the results are well constrained by the data.

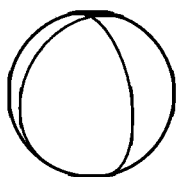
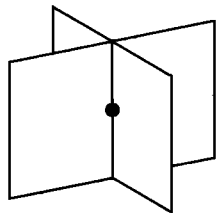
Method

The MSE algorithm determines an earthquake's mechanism from a suite of observed seismograms, using methods from the theory of optimal filter design. The moment tensor of the source is regarded as an unknown multichannel filter whose input is a set of Green's functions and whose output is a set of theoretical seismograms. The input Green's functions are taken as known, and the algorithm determines the filter (moment tensor) that makes the output agree as well as possible with the observed seismograms. The moment tensor acts as both a signal enhancement filter and a noise rejection filter; features of the seismograms that are not included in the Green's functions (for example, arrivals generated by unmodeled near-receiver or near-source structure) are regarded as noise and have little effect on the solution. The MSE waveform inversion algorithm has the advantages of being more objective (and much faster) than trial and error methods and is less sensitive to lateral heterogeneity in earth structure than are techniques that use long portions of the wave train.

We used two variants of the MSE algorithm. In the first variant, all the components of the moment tensor are constrained to be similar functions of time, differing only by constant factors, while in the second variant the components are allowed to be independent functions of time. This second representation provides information about the time history of the rupture process and is helpful for identifying multiple earthquakes and for studying such processes as changes in fault orientation or in slip direction. For example, for the Coalinga, California, earthquake of May 2, 1983, a rotation of the fault plane by about 10° was easily resolvable.

NODAL SURFACES

QUADRANTAL



CONICAL

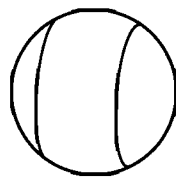
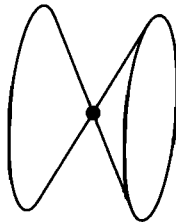


Fig. 5. (Top) P wave nodal surfaces for double-couple (left) and CLVD (right) earthquake mechanisms. (Bottom) Intersections of nodal surfaces with focal sphere.

The MVD method was developed by Oldenburg [1982] and is based on Backus-Gilbert inverse theory. This method generates smoothed time domain versions of the components of the moment rate tensor such that all solutions satisfying the data within a given accuracy have the same averages. It also gives quantitative estimates of accuracy and temporal resolution, including explicit information about the trade-off between these two quantities. The method's advantage is that it estimates the uniqueness of its results. Its main drawback is that it requires a certain amount of interaction and is not easily automated.

In all the waveform inversions the solutions were constrained to be purely deviatoric but were not required to be double couples. The Green's functions used are those for the far field of a point source, computed by the WKB method, and include the effects of reflection at the free surface, anelastic attenuation, and instrument response.

The inversion was carried out in several steps. First, to estimate the focal depths, we inverted *P* waveforms using the MSE algorithm, with the moment tensor components constrained to be similar time functions, and varied the depth until the best fit to the data was obtained. Figure 6 shows the variation of the mean squared error with depth for event 3. Since the *P* waveforms contain the phases *pP* and *sP*, as well as the direct *P* waves, this procedure is sensitive to source depth. We then constrained the depth to the best fitting value and performed MVD inversions using *P* and *SH* waveforms. Finally, for the events with large non-double-couple components (events 1 and 3), we did the more general type of MSE *P* wave inversion, dropping the similarity restriction on the moment tensor components.

Results

The waveform inversion techniques were applied to *P* and *SH* wave GDSN data recorded at epicentral distances from 52° to 99° (Figure 7) for events 1, 2, and 3. The source depths determined for the three events are 9, 11, and 7 km, respectively. For events 1 and 3, inversions were done using *P* waves alone and using *P* and *SH* waves together. For event 2 there were not enough suitable *P* waves, so only a *P-SH* inversion was done. The *P* inversions were done using the MSE algorithm, and the *P-SH* inversions were done using the MVD algorithm. The resulting moment tensors are listed in Table 2 and shown in Figure 1. The fits of the resultant theoretical waveforms to the data for the three events are shown in Figures 8, 9, and 10. For events 1 and 3 the scalar moments

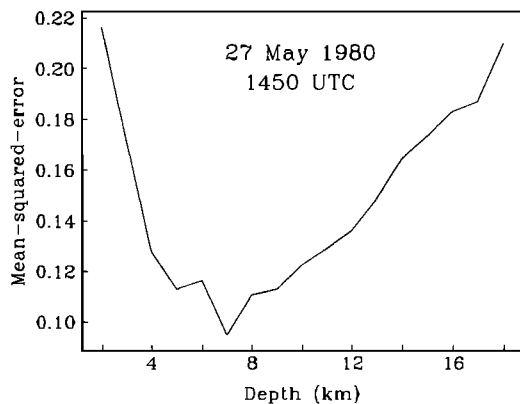


Fig. 6. Mean squared error versus assumed focal depth from MSE inversion for event 3.



Fig. 7. Azimuthal equidistant projection, centered on Long Valley caldera and showing the GDSN stations used in waveform inversions. The edge of the map is at an epicentral distance of 100°.

(defined as half the algebraic difference between the extreme principal moments) are 2.3×10^{18} and 1.3×10^{18} N m, corresponding to magnitudes M_w of 6.2 and 6.0. The double-couple parts of the moment tensors are 52 and 57%. However, the solution for event 2 is almost a pure double couple, with a non-double-couple part of only 5% and a scalar moment of 1.2×10^{18} N m ($M_w = 6.0$).

For comparison, Table 2 also shows the moment tensors computed for events 1 and 3 by Barker and Langston [1983], who inverted long-period WWSSN waveforms. (The plunges and trends are taken directly from their Table 5. The principal moments are calculated from the moment tensor components. Note that in Barker and Langston's table the M_{12} value for event 3 has a misplaced decimal point; the correct value is -0.584 .) The agreement between their results and ours, partic-

TABLE 2. Moment Tensors

Event	Method	Principal Moments, 10^{18} N m	Principal Axes		
			Trend	Plunge	CLVD
1	MSE(P)	2.12	237°	7°	59%
		-0.63	137°	55°	
		-1.50	331°	34°	
	MVD(P, SH)	2.59 ± 0.09	67°	3°	48%
		-0.62 ± 0.09	178°	83°	
		-1.96 ± 0.11	336°	7°	
BL	2.12	244°	10°	61%	
	-0.65	137°	58°		
	-1.46	340°	30°		
2	MVD(P, SH)	1.22 ± 0.18	231°	16°	5%
		0.03 ± 0.11	18°	71°	
		-1.24 ± 0.19	138°	10°	
3	MSE(P)	1.40	248°	11°	60%
		-0.42	104°	77°	
		-0.98	339°	8°	
	MVD(P, SH)	1.47 ± 0.15	64°	6°	43%
		-0.31 ± 0.19	156°	18°	
		-1.15 ± 0.14	317°	71°	
BL	1.15	249°	13°	61%	
	-0.35	129°	64°		
	-0.80	344°	21°		

BL, Barker and Langston [1983].

25 May 1980
16:33 UTC

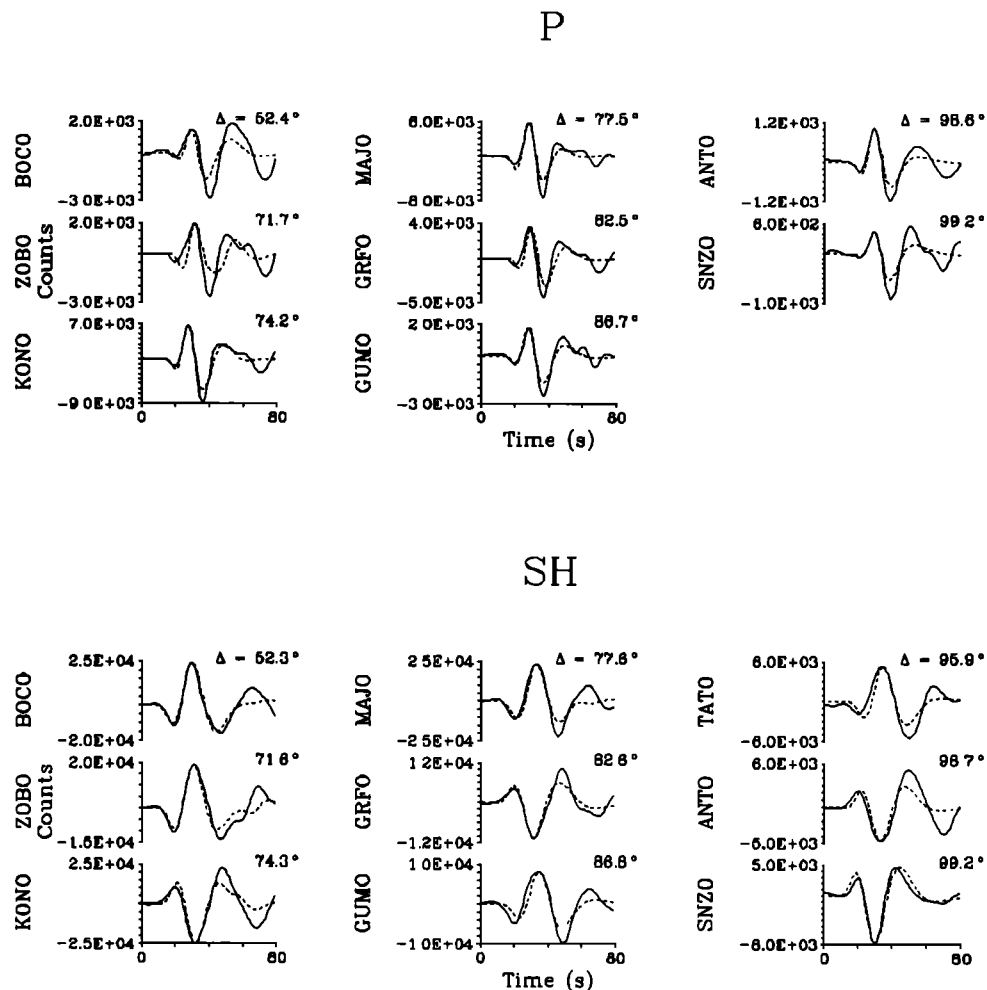


Fig. 8. Real (solid) and synthetic (dashed) waveforms for event 1.

ularly those derived by the MSE method, is good. The largest principal moments, corresponding to the tension axes, are practically the same for all three results. The slightly larger difference for the other two axes is to be expected because their directions become inherently less well determined as their principal moments become more nearly equal. (In the degenerate case of a pure CLVD these axes must lie in the plane normal to the T axis but are otherwise undetermined.) The agreement between our results and those of Barker and Langston, which were derived from different data and by different analysis methods, is strong evidence that the non-double-couple components of the mechanisms are well resolved.

The result of the general MSE inversion for event 1, without a similarity constraint on the moment tensor components (and of the MVD inversion), is a moment tensor with a large non-double-couple component at all times; the earthquake is not composed of double-couple subevents. The source time function (scalar moment as a function of time) is shown in Figure 11. Event 1 has a duration of about 20 s and consists of three distinct subevents. The first two of these can be detected vis-

ually on both near-field strong motion records, discussed above, and on broadband waveforms, which will be discussed in more detail below. Event 3, also shown in Figure 11, consists of a single event, with no evidence of multiplicity, a conclusion that is also in accord both with Hartzell's [1982] strong-motion seismograms and with broadband waveforms, discussed below. The source time functions for both events 1 and 3 agree well with those computed by Barker and Langston [1983] from WWSSN data. As in the case of the moment tensors, this fact argues strongly that these time functions are well resolved.

The MVD algorithm generates standard error estimates for the principal moments, from which we can estimate how well the mechanism is determined. These are given in Table 2. For an event to be a double couple it would be necessary that the intermediate principal moment have a true value of zero. This hypothesis can be rejected at an extremely high confidence level for event 1 and at a considerable lower level for event 3. The formal confidence level (about 99.99999999%) is based on the assumption of independent, normally distributed random errors and is undoubtedly too optimistic; clearly,

25 May 1980
19:44 UTC

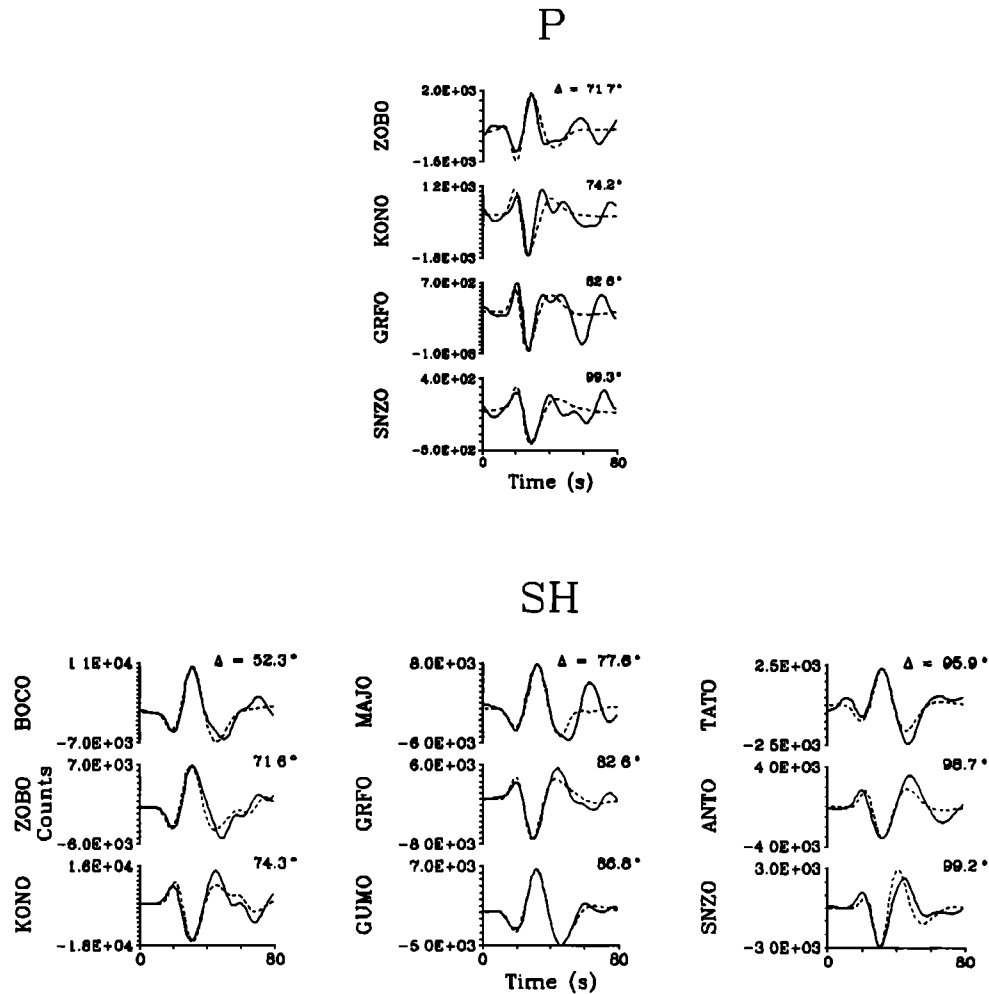


Fig. 9. Real (solid) and synthetic (dashed) waveforms for event 2.

however, the non-double-couple nature of the moment tensor is well resolved.

The temporal resolution of the source time functions depends on the station distribution, the character of the noise and the bandwidth of the instrument. The MVD algorithm generates a set of averaging functions, which quantitatively specify this resolution, a typical one of which is shown in Figure 12 (computed for event 1 and the *P-SH* data set). Its width is about 6 s; subevents separated by less than this interval can not be resolved. That events about 8 s apart were clearly resolved for event 1 is evidence that this estimate of the resolution is realistic.

SURFACE WAVES

As was pointed out above, the Long Valley earthquakes are so shallow that their surface waves provide information about only three of the six moment tensor components. As a result, the observed surface wave spectral amplitudes and initial phases can be explained equally well by many different mechanisms, including a pure double couple and a pure CLVD. It is nevertheless worthwhile to verify that any proposed mechanism is quantitatively consistent with the observed surface

waves. Event 1 provides the most stringent test because it has the largest seismic moment and generated the highest-quality surface wave data. Figure 13 shows the observed spectral amplitudes of 197-s Love and Rayleigh waves for this event and compares them with the theoretical radiation patterns for the double-couple mechanism proposed by *Given et al.* [1982] and for the two non-double-couple mechanisms determined in this study by inverting *P* and *SH* waveforms. The observed and theoretical radiation patterns for 150-s period waves are much like the 197-s results shown in Figure 13. All three theoretical radiation patterns are similar. As expected, the solution of *Given et al.* [1982], which was derived from these surface wave data, fits them the best. The body wave solutions fit about as well as would be expected for solutions derived from different types of waves separated by one decade in frequency. The MVD solution, derived from *P* and *SH* waves, fits better than the MSE solution, which is based upon *P* waves only. In fact, the MVD solution agrees with the surface wave data better than the two body wave solutions agree with each other. Because the two body wave solutions predict significantly different surface wave radiation, it is clear that the surface waves, although not powerful enough to establish whether an event is

27 May 1980
14:50 UTC

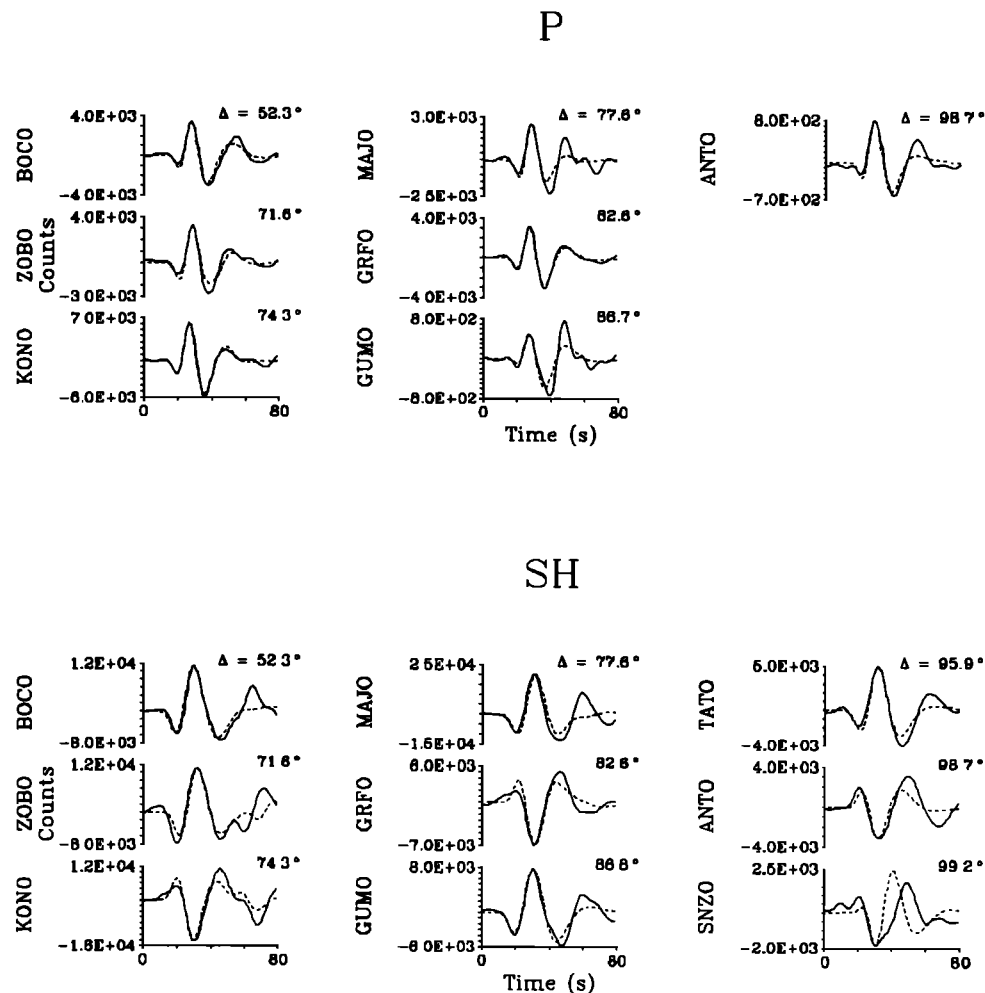


Fig. 10. Real (solid) and synthetic (dashed) waveforms for event 3.

a double couple, do provide useful information that is not contained in the P and SH waveforms. Inverting all the data simultaneously would probably yield a mechanism that fits both data sets well, but it is not certain that such a solution would be a truer representation of the earthquake's mechanism. Because the resolution of both data sets is finite, there would remain the possibility that the mechanism is frequency dependent in the 0.005–0.05 Hz band.

BROADBAND WAVEFORMS

Long-period seismograms, recorded on narrow-band instruments, are poorly suited for assessing the complexity of the source process. Records from broadband instruments are much better for this purpose, but few such instruments are now deployed. However, if digital waveforms of high resolution and accuracy are available, it is possible to combine outputs from short- and long-period instruments to synthesize seismograms of increased bandwidth. Such broadband signals are powerful for recognizing subevents within an earthquake, as well as for identifying the depth phases pP and sP .

We used the technique described by *Harvey and Choy* [1982] to produce broadband seismograms from data record-

ed by the Global Digital Seismograph Network (GDSN). Figures 14 and 15 show the broadband displacements from events 1 and 3. The broadband waveforms for event 3 are extremely simple, with an initial dilatation followed by a somewhat larger and broader compressional arrival. The initial arrival is the direct P wave, and the later arrival is a combination of pP and sP (and PcP at station GRFO). There is no evidence in the broadband waveforms of any source multiplicity.

The waveforms for event 1 (Figure 14) are considerably more complex. By comparing these waveforms with the simpler ones for the earthquake 2 days later, it is possible to identify two events about 6–8 s apart, as was suggested by *Given et al.* [1982] (who estimated the interval to be 4 s), *Ekström and Dziewonski* [1983], and *Ekström* [1983]. Evidence of these two subevents can also be seen in the near-field strong motion records displayed by *Hartzell* [1982]. *Ekström* [1983] and *Wallace et al.* [1983] argued that these subevents have different mechanisms, by whose superposition they sought to explain the non-double-couple mechanism of the earthquake. *Ekström's* analytical technique was to specify a normal-faulting mechanism for the first event and then determine the second (strike slip) so as to obtain the correct result-

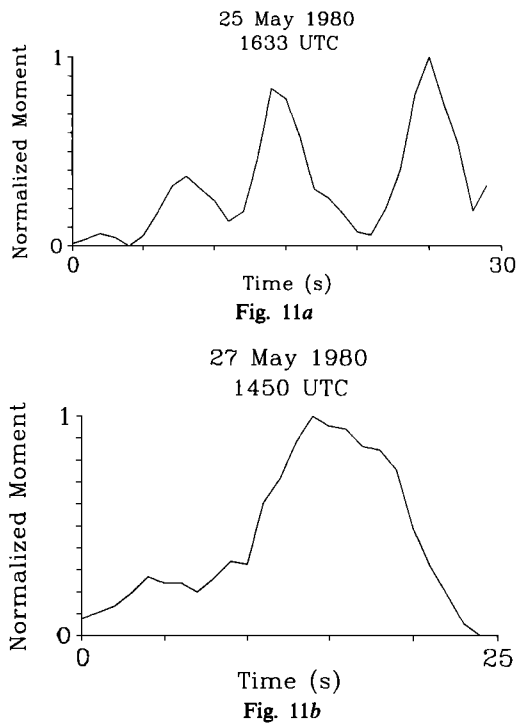


Fig. 11. Source time functions (scalar moment as a function of time): (a) event 1; (b) event 3.

ant moment tensor. As was mentioned above, such a mathematical decomposition of a moment tensor is always possible and is not unique. Ekström's interpretation is not required by the data; Wallace *et al.* [1983] explain the same data with a strike-slip event followed by a normal-faulting event. Objective inversion of the waveforms, discussed above, shows that the mechanism has a large non-double-couple component at all times.

The later phases on the broadband records can be used to determine the depth of focus for event 3. The intervals between the arrival times of the initial dilatations, and the following compressions fall into two groups, averaging about 4.4 and 6.1 s. If the first group represents the *pP-P* times and the second group represents the *sP-P* times and if the crustal compressional and shear wave speeds are about 6.0 and 3.3 km/s, then the source depth is about 12.6 km. Of course, the effect of any low-velocity surficial layers will be to decrease this estimate and make the earthquake shallower. The depth found is close to the 13-km depth determined by the National Earthquake Information Service and to the 10 km depth obtained from local and regional observations. These depths are significantly greater than the 7-km centroidal source depth determined from long-period body wave inversion, which suggests that the source probably propagated upward.

AFTERSHOCK LOCATIONS

The orientation of fault planes defined by aftershock locations has great potential power to distinguish between shear and tensile failure modes. At Long Valley the smallest (least compressive) principal stress axis, as inferred from the orientation of normal faults, the tensional axes of earthquake focal mechanisms [Vetter and Ryall, 1983], and geodetically observed deformation [Savage and Lisowski, 1984], is approximately horizontal and trends in the direction N65°E. Consequently both strike-slip and tensile faults are expected to be

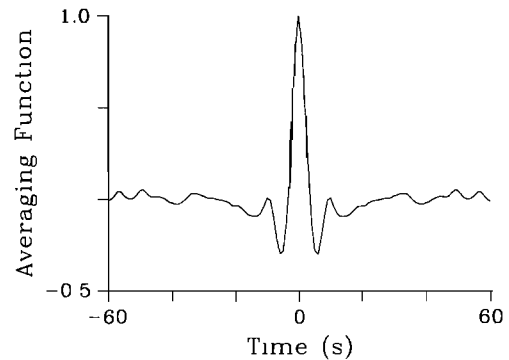


Fig. 12. Averaging function for the $M_{\phi\phi}$ component of the moment tensor for event 1.

approximately vertical, with strike-slip faults striking slightly east of north and tensile faults striking about 335°. Normal faults would also strike about 335° but instead of being vertical would dip about 60° to the northeast or southwest. If the non-double-couple earthquakes are caused by tensile failure, their failure surfaces, as determined from aftershock locations, should be diagnostic of this fact.

The Long Valley earthquakes since 1978 are distributed in a complex pattern throughout a large volume in the southern part of the caldera and in the Sierra Nevada south of the caldera. Unfortunately, the seismological data available vary greatly in quality and quantity over this period. Coverage is most complete and location estimates are most accurate for the period since mid-1982, when a dense seismograph network was installed by the U.S. Geological Survey. Data available for the period before this, from sparser regional networks and from temporary experiments conducted by various agencies, are less complete and have poorer resolving power for hypocenter estimation. Location estimates for about 900 well-located earthquakes between June 1982 and July 1984 have

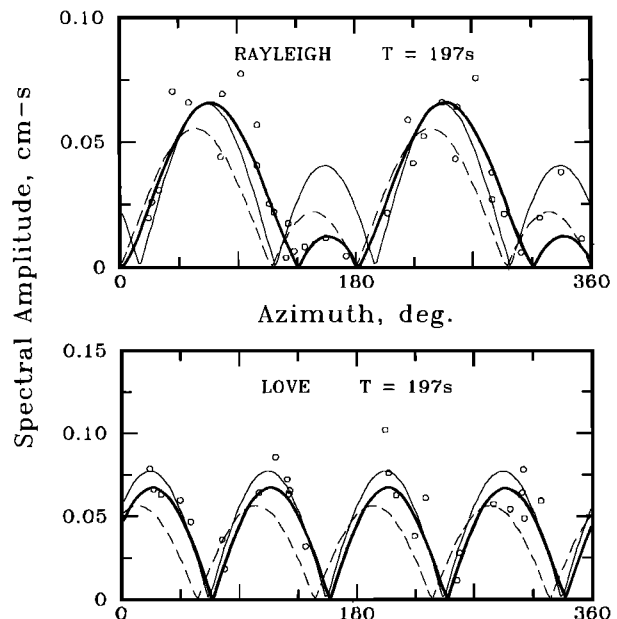


Fig. 13. Observed and predicted 197-s surface wave amplitudes for earthquake 1. Heavy lines, theoretical amplitudes for shear fault with strike 12°, dip 50° and rake -35° ("solution 2" of Given *et al.* [1982]). Light lines, theoretical amplitudes for MVD(*P*, *SH*) solution. Dashed lines, theoretical amplitudes for MSE(*P*) solution.

25 May 1980 16:33

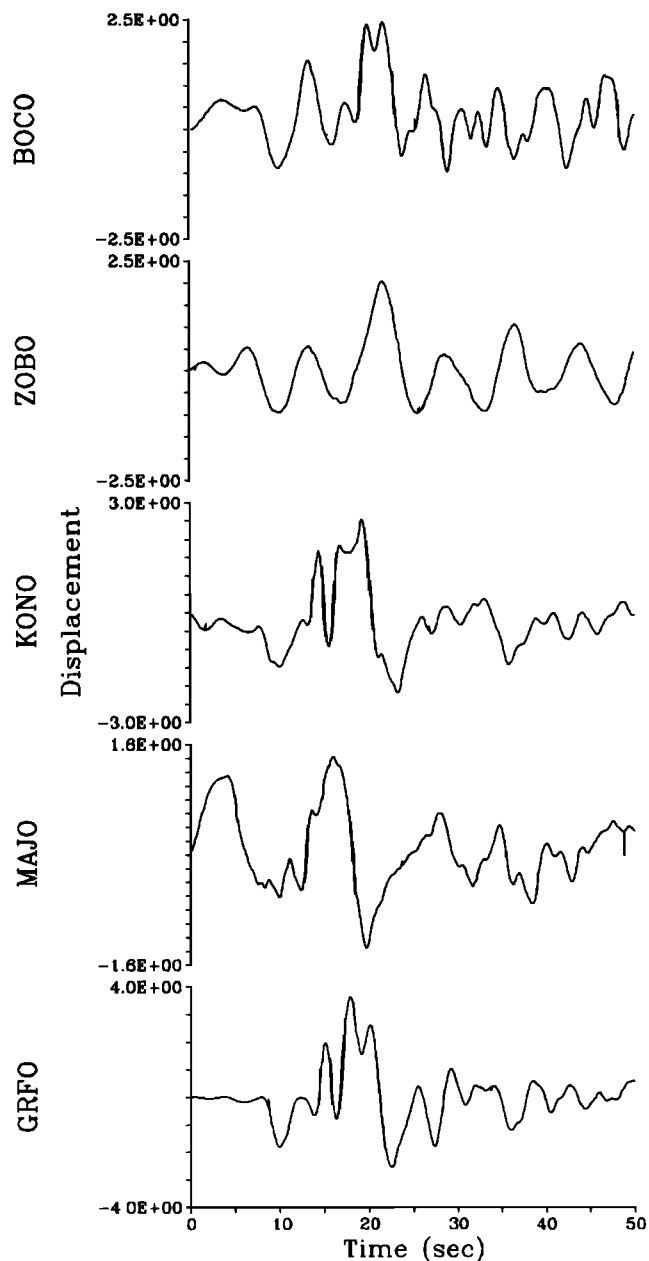


Fig. 14. Broadband displacement waveforms for event 1.

been studied by *Cockerham and Pitt* [1984]. In map view the pattern of the epicenters of these earthquakes appears complex and shows features with a variety of trends, ranging from NNE-SSW to NW-SE. The NNE-SSW alignments are similar to those of earthquakes in 1980, which *Lide and Ryall* [1984] interpreted as left-lateral strike-slip faults. At least for the 1982–1984 earthquakes, however, most of these alignments are caused by nonuniform distributions of earthquakes on planes with whose strikes are quite different from the trends seen in map view. Vertical cross-section plots of the hypocenters show that most of the earthquakes with NNE-SSW trends in map view actually lie on well-defined planes striking approximately NNW-SSE. Thus the most definite spatial patterns in these earthquakes strike NNW-SSE in the direction appropriate for normal or tensile faults.

One of the most prominent NNW-SSE alignments is a nearly vertical plane that has the position and orientation expected for the tensile-failure of the largest May 1980 earthquake (event 1). Before this feature can be conclusively identified, however, a more complete and accurate catalog of the 1980 aftershocks is needed. It may be possible to obtain such a catalog by merging data gathered by different institutions and processing them specially, for example, by using three-dimensional structural models that are now available for the area [*Kissling et al.*, 1984]. If it turns out that this plane is evident in the immediate aftershocks of event 1, especially in the region close to the hypocenter, it will constitute strong evidence that earthquake 1 was caused by tensile failure.

DISCUSSION

What type of focal mechanism would one expect for a rapidly running tensile crack? At depth a void cannot form, and a tensile crack can open only if fluid under high pressure flows into it and holds it open. Indeed, if the fluid pressure is high enough, tensile failure is the only type of failure that can occur (Figure 16). A simple qualitative argument shows that the focal mechanism of such a process must have a large CLVD component. The equivalent force system for a shear fault is a double couple, whose principal axis representation is a pair of orthogonal dipoles of equal magnitude and opposite sign. A CLVD, on the other hand, consists of three dipoles, with moments in the ratio 2 : -1 : -1. Now an opening tensile crack may be represented as a plane across which there is a discontinuity in the normal component of displacement; the equivalent force system consists of three dipoles with moments in the ratio $\lambda + 2\mu : \lambda : \lambda$ [*Aki and Richards*, 1980]. If we add an implosive force system that is symmetric about the primary (extensional) dipole and just cancels out the volumetric component, as is required by the fact that large voids cannot form at depth in the earth, we obtain a CLVD. Physically, the compensation is provided by fluid flowing into the crack and would not be completely symmetric, so the resultant force system would not be a pure CLVD but would also have a double-couple component. This type of earthquake mechanism was originally proposed in Japan more than 50 years ago by *Ishimoto* [1932], who attributed most earthquakes to magma movement.

Conditions for Tensile Failure

Under what conditions will tensile failure occur, as opposed to shear failure? This question can be conveniently analyzed using a Mohr's circle diagram, shown in Figure 16. Only the general shape of the failure envelope is important in this discussion. If the mean stress is large and fluid pressure is unimportant, as in the upper part of Figure 16, only shear failure can occur. The approximate effect of a fluid pressure p is to effectively lower the principal stresses by the amount p . If the fluid pressure is comparable to the overburden pressure, the effective confining stress becomes small, and tensile failure can occur for small stress differences. The restrictive nature of this condition on fluid pressure probably explains why tensile failure in the earth is apparently rare.

Volume of the Intrusion

The volume V of fluid intruded into a crack is related to the seismic moment of the associated earthquake. If we assume that the equivalent forces for the fluid flow are confined to the plane of the crack, then these forces do not affect the principal dipole of the CLVD normal to the crack, whose moment is

$$M = (\lambda + 2\mu)A\bar{u} \equiv (\lambda + 2\mu)V$$

27 May 1980 14:50

MODES OF FAILURE

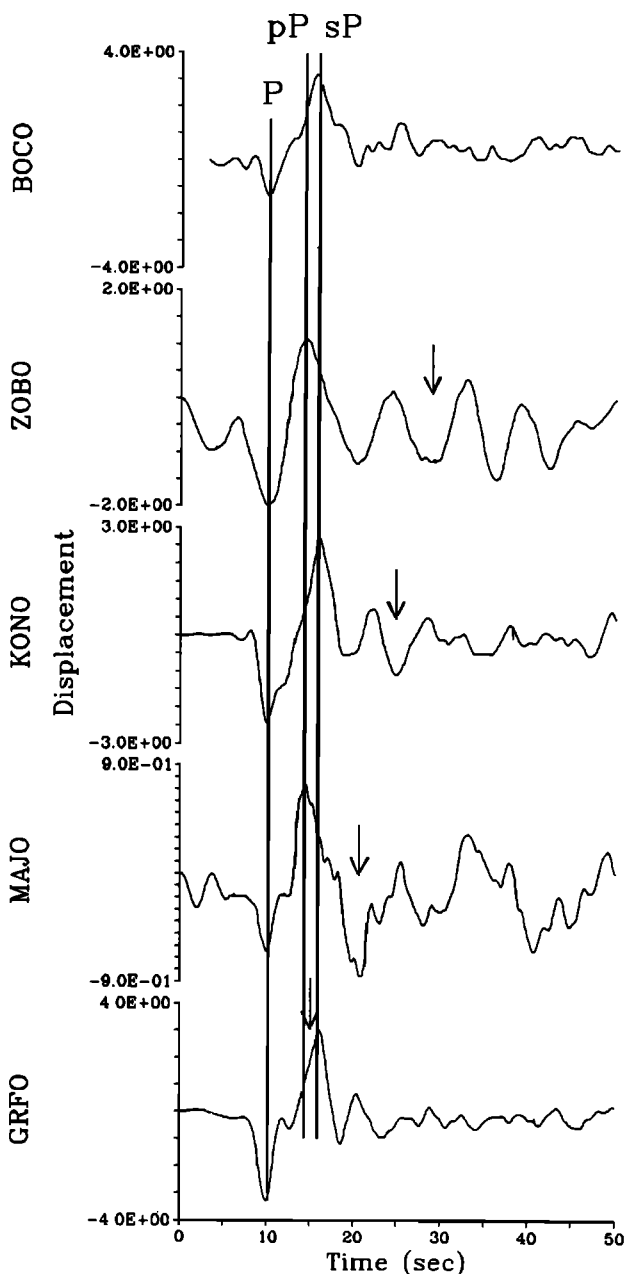


Fig. 15. Broadband displacement waveforms from event 3. Vertical lines, peaks of the P, pP, and sP arrivals. Arrows, computed PcP times (peak of arrival).

where A is the area of the crack face and \bar{u} is the average amount of opening of the crack. For the largest earthquake, event 1, $M = 1.7 \times 10^{18}$ N m. Taking $\lambda = \mu = 3 \times 10^{10}$ N m⁻², we get $V = 1.8 \times 10^7$ m³.

The distributions of observed ground breakage and aftershocks, discussed above, suggest that the crack that caused earthquake 1 had dimensions of about 12 km \times 6 km, so the inferred volume implies an opening of about 0.25 m. These figures represent an upper bound on the crack dimensions and a lower bound on the amount of opening because several days of intense aftershock activity elapsed between the earthquake and the field observations, during which time the ground breakage may have spread. The opening varies inversely with the square of the linear dimensions of the crack; if these di-

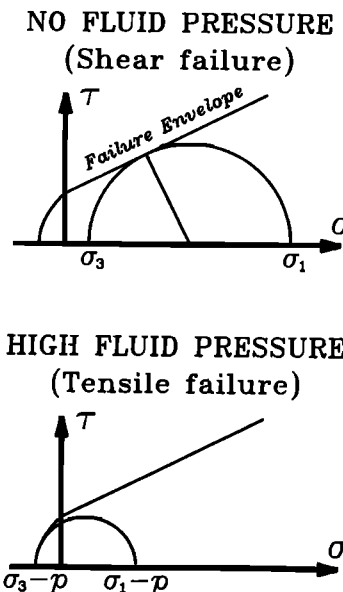


Fig. 16. Conditions for shear and tensile failure. Mohr's circle diagram shows the relationship between shear traction τ and normal traction σ across a plane at a point in a stressed medium. Locus of (σ, τ) points for different orientations of plane is a circle of diameter $\sigma_1 - \sigma_3$, centered at $[(\sigma_1 + \sigma_3)/2, 0]$. Failure occurs when circle touches "failure envelope." (Theoretical failure envelope shown corresponds to Griffith theory of failure, as modified by F. A. McClintock and J. B. Walsh [Price, 1966].) Straight portion of failure envelope in compressional field ($\sigma > 0$) represents the Navie-Coulomb criterion for shear failure. (Top) At high confining stress with no fluid pressure, only shear failure occurs. (Bottom) High fluid pressure lowers the effective confining stress, and tensile failure occurs at low stress differences.

mensions are reduced by a factor of 2, the inferred opening becomes 1 m.

Fluid Viscosity

It might be thought that some fluids, such as magma, are too viscous to flow into a crack fast enough to cause an earthquake. Approximate calculations show that this is not necessarily so. Consider a dike of thickness h , horizontal length l , and vertical aspect ratio r propagating upward from a source of magma or other high-pressure fluid. The volume of the dike is

$$V = rh^2l$$

and for laminar viscous flow the flow rate is

$$\dot{V} = \frac{lh^3}{12\eta} \frac{dP}{dx} = \frac{lh^3}{12\eta} \frac{\Delta P}{rh} = \frac{V\Delta P}{12r^2\eta}$$

The pressure difference driving the fluid into the crack, ΔP , is comparable in magnitude to the strength of the rock for new fractures and is considerably less for preexisting fractures. From the above equation it follows that V varies as $\exp(t/\tau)$, where

$$\tau = 12r^2\eta/\Delta P$$

The crack volume increases exponentially, with a time constant that depends on the driving pressure, the shape of the crack, and the viscosity of the fluid. Of course the crack can not grow indefinitely; the analysis given here ignores effects

such as the dynamics of rock failure and the pressure drop in the source reservoir, which would limit crack growth. If we take $\tau = 20$ s, the approximate duration of earthquake 1, $r = 100$ to 1000, the approximate range observed for exhumed dikes, and $\Delta P = 10$ to 100 MPa (100–1000 bars), we get values for η between 17 and 1.7×10^4 N s m⁻² (170 and 1.7×10^5 P), a range that overlaps the viscosities observed for many magmas. If, on the other hand, we use $r = 2.4 \times 10^4$, in keeping with the upper bounds on crack dimensions inferred above, we get $\eta < 0.3$ N s m⁻² (3 P), a value too low for magma. (It should be remembered that the aspect ratio inferred here is proportional to the cube of the linear crack dimensions and therefore has a large uncertainty. The viscosity depends on the square of the aspect ratio and is even more uncertain.) This argument shows that magma intrusion rapid enough to cause earthquakes can not be ruled out on the basis of viscosity if we assume crack dimensions like those of dikes now exposed to view but that it can be ruled out if the large aspect ratio inferred for event 1 is correct. In either case, other fluids such as water or carbon dioxide remain equally acceptable possibilities. Indeed, the rapid exsolution of such volatile fluids after a drop in pressure is likely to be an important mechanism increasing the mobility of magma.

Dynamics of Tensile Failure

The argument given above for a CLVD component in the mechanism of a tensile earthquake is highly qualitative. It is important to develop more quantitative models of the dynamic behavior of such a seismic source and to compare them with observed seismograms. Chouet and Julian [this issue] have developed a finite difference numerical model of the motion resulting from a sudden propagation of the tip of a fluid-filled crack in a infinite homogeneous medium. A preliminary evaluation of their results suggests that this model probably can not explain the Long Valley earthquakes. In particular, the model predicts that all first motions are compressional, and it cannot explain the dilatations observed at some stations. This model still needs refinement, however, to account for such effects as seismograph response and anelastic attenuation. In addition, similar modeling is needed to evaluate other possibilities, such as cracks propagating outward from a magma reservoir. Another important question is whether a tensile crack at depth could propagate rapidly enough to radiate seismic waves. Most earlier workers, such as Aki *et al.* [1977], have assumed that it could, although simple arguments based on stress intensity factors suggest that such cracks should propagate stably.

Non-double-couple earthquake mechanisms have sometimes been reported from other areas of volcanism and extensional tectonics. For example, it is often impossible to fit orthogonal model planes to P wave first motions from large "normal faulting" earthquakes on the Mid-Atlantic Ridge [Sykes, 1967, 1970]. This difficulty was at one time attributed to wave refraction by low-velocity structures beneath the ridge [Solomon and Julian, 1974], but the anomalous mechanisms are now thought to be an artifact of ignoring the pP and sP phases in interpreting first motions [Trehu *et al.*, 1981]. Examples of anomalous mechanisms similar to those discussed here have recently been reported for small earthquakes at the Hengill geothermal area in Iceland [Foulger and Long, 1984]. It would be worthwhile to reexamine earthquakes from other volcanic areas to see if anomalous mechanisms have been overlooked.

CONCLUSIONS

At least three of the largest Long Valley earthquakes have unusual non-double-couple focal mechanisms, unlike those appropriate for slip on faults. Simple double couples are not capable of explaining the seismic data, which include short-period P first motions, long-period P and SH first motions, surface wave spectral amplitudes and initial phases, and long-period P and SH waveforms. The suggestion that these earthquakes are complex events, caused by simultaneous slip on different faults, and that the non-double-couple mechanisms are artifacts caused by failure to resolve the separate events is inconsistent with the observed P and SH waveforms. Although the largest earthquake (event 1) has a complex source time function that can be resolved into three distinct sub-events, these subevents themselves have non-double-couple mechanisms. This situation contrasts sharply with most other complex earthquakes with apparent non-double-couple mechanisms, which are found to consist of double-couple subevents. Furthermore, one earthquake (event 3) has a simple source time function unlike that expected for a multiple event.

The most likely physical explanation of these earthquakes is that they are caused by sudden tensile failure and the opening of cracks under high fluid pressure. If this explanation is correct, earthquake mechanisms may prove useful for monitoring intrusive processes in active volcanic areas.

Acknowledgments. During this study we had valuable conversations with David Hill, William Ellsworth, James Savage, and Rob Cockerham. We thank Rob Cockerham for permission to use unpublished data, Terry Wallace for giving us surface wave spectral data, Peter Ward for help in digitizing published data, and Madeleine Zirbes for help in retrieving and processing digital seismic data.

REFERENCES

- Aki, K., and P. G. Richards, *Quantitative Seismology*, 932 pp., W. H. Freeman, San Francisco, Calif., 1980.
- Aki, K., M. Fehler, and S. Das, Source mechanism of volcanic tremor: Fluid-driven crack models and their application to the 1963 Kilauea eruption, *J. Volcanol. Geotherm. Res.*, 2, 259–287, 1977.
- Barker, J. S., and C. A. Langston, A teleseismic body-wave analysis of the May 1980 Mammoth Lakes, California, earthquakes, *Bull. Seismol. Soc. Am.*, 73, 419–434, 1983.
- Chouet, B., and B. R. Julian, Dynamics of an expanding fluid-filled crack, *J. Geophys. Res.*, this issue.
- Clark, M. M., J. C. Yount, P. R. Vaughan, and R. L. Zepeda, Map showing surface ruptures associated with the Mammoth Lakes, California, earthquakes of May 1980, *U.S. Geol. Survey Misc. Field Stud.*, Map MF-1396, 1982.
- Cockerham, R. S., and A. M. Pitt, Seismic activity in Long Valley caldera, eastern California, U.S.A.: June 1982 through July 1984, Active Tectonic and Magmatic Processes Beneath Long Valley Caldera, Eastern California, *U.S. Geol. Surv. Open File Rep.*, 84-939, 493–526, 1984.
- Cramer, C. H., and T. R. Topozada, A seismological study of the May, 1980, and earlier earthquake activity near Mammoth Lakes, California, *Spec. Rep. Calif. Div. of Mines and Geol.*, 150, 91–130, 1980.
- Eaton, J. P., Crustal structure from San Francisco, California, to Eureka, Nevada, from seismic-refraction measurements, *J. Geophys. Res.*, 68, 5789–5806, 1963.
- Ekström, G., Evidence for source complexities of 1980 Mammoth Lakes earthquakes (abstract), *Eos Trans. AGU*, 64, 769, 1983.
- Ekström, G., and A. M. Dziewonski, Moment tensor solutions of Mammoth Lakes earthquakes (abstract), *Eos Trans. AGU*, 64, 262, 1983.
- Foulger, G., and R. E. Long, Anomalous focal mechanisms: Tensile crack formation on an accreting plate boundary, *Nature*, 310, 43–45, 1984.

- Given, J. W., T. C. Wallace, and J. Kanamori, Teleseismic analysis of the 1980 Mammoth Lakes earthquake sequence, *Bull. Seismol. Soc. Am.*, **72**, 1093-1109, Aug 1982.
- Hartzell, S., Simulation of ground accelerations for the May 1980 Mammoth Lakes, California, earthquakes, *Bull. Seismol. Soc. Am.*, **72**, 2381-2387, 1982.
- Harvey, D., and G. L. Choy, Broadband deconvolution of GDSN data, *Geophys. J. R. Astron. Soc.*, **69**, 659-668, 1982.
- Ishimoto, M., Existence d'une source quadruple au foyer sismique d'après l'étude de la distribution des mouvements initiaux des secousses sismiques, *Bull. Earthquake Res. Inst. Univ. Tokyo*, **10**, 449-471, 1932.
- Johnson, L. R., Crustal structure between Lake Mead, Nevada and Mono Lake, California, *J. Geophys. Res.*, **70**, 2863-2872, 1965.
- Julian, B. R., Evidence for dyke intrusion earthquake mechanisms near Long Valley caldera, California, *Nature*, **303**, 323-325, 1983.
- Julian, B. R., Analysis of seismic-source mechanisms by linear-programming methods, *Geophys. J. R. Astron. Soc.*, in press, 1985.
- Kissling, E., W. L. Ellsworth, and R. S. Cockerham, Three-dimensional structure of the Long Valley caldera, California, region by geotomography, Active Tectonic and Magmatic Processes Beneath Long Valley Caldera, Eastern California, *U.S. Geol. Surv. Open File Rep.*, **84-939**, 188-220, 1984.
- Knopoff, L., and M. J. Randall, The compensated linear-vector dipole: A possible mechanism for deep earthquakes, *J. Geophys. Res.*, **75**, 4957-4963, 1970.
- Lide, C. S., and A. S. Ryall, Relationship between aftershock locations and mechanisms of the May, 1980 Mammoth Lakes earthquakes, Active Tectonic and Magmatic Processes Beneath Long Valley Caldera, Eastern California, *U.S. Geol. Surv. Open File Rep.*, **84-939**, 440-452, 1984.
- Oldenburg, D. W., Multichannel appraisal deconvolution, *Geophys. J. R. Astron. Soc.*, **69**, 405-414, 1982.
- Price, N. J., *Fault and Joint Development in Brittle and Semi-Brittle Rock*, 176 pp., Pergamon, New York, 1966.
- Ryall, A., and F. Ryall, Spatial temporal variations in seismicity preceding the May 1980, Mammoth Lakes, California, earthquakes, *Bull. Seismol. Soc. Am.*, **71**, 747-760, Jun 1981.
- Savage, J. C., and M. Lisowski, Deformation in the White Mountain seismic gap, California-Nevada, 1972-1982, *J. Geophys. Res.*, **89**, 7671-7687, 1984.
- Sipkin, S. A., Estimation of earthquake source parameters by the inversion of waveform data: Synthetic waveforms, *Phys. Earth Planet. Inter.*, **30**, 242-259, 1982.
- Solomon, S. C., and B. R. Julian, Seismic constraints on ocean-ridge mantle structure: Anomalous fault-plane solutions from first motions, *Geophys. J. R. Astron. Soc.*, **38**, 265-285, 1974.
- Sykes, L. R., Mechanism of earthquakes and nature of faulting on the mid-oceanic ridges, *J. Geophys. Res.*, **72**, 2131-2153, 1967.
- Sykes, L. R., Focal mechanism solutions for earthquakes along the world rift system, *Bull. Seismol. Soc. Am.*, **60**, 1749-1752, 1970.
- Taylor, G. C., and W. A. Bryant, Surface rupture associated with the Mammoth Lakes earthquakes of 25 and 27 May, 1980, *Spec. Rep. Calif. Div. Mines Geol.*, **150**, 49-67, 1980.
- Trehu, A. M., J. L. Nabelek, and S. C. Solomon, Source characterization of two Reykjanes Ridge earthquakes: Surface waves and moment tensors, *P waveforms and nonorthogonal nodal planes*, *J. Geophys. Res.*, **86**, 1701-1724, 1981.
- Vetter, U. R., and A. S. Ryall, Systematic change of focal mechanism with depth in the western Great Basin, *J. Geophys. Res.*, **88**, 8237-8250, 1983.
- Wallace, T., J. Given, and H. Kanamori, A discrepancy between long- and short-period mechanisms of earthquakes near the Long Valley Caldera, *Geophys. Res. Lett.*, **9**, 1131-1134, 1982.
- Wallace, T. C., L. J. Burdick, and H. Kanamori, Faulting and crustal structure complexity: A possible explanation for the moment tensor solutions of the 1980 Mammoth Lakes earthquakes (abstract), *Eos Trans. AGU*, **64**, 769, 1983.

B. R. Julian, U.S. Geological Survey, 345 Middlefield Road, MS/977, Menlo Park, CA 94025.

S. A. Sipkin, U.S. Geological Survey, Box 25046, MS/967, Denver Federal Center, Denver, CO 80225.

(Received July 26, 1984;
revised March 21, 1985;
accepted March 26, 1985.)